[5] Fundamentals Of Physics 9th edition/ David Halliday, Robert Resnick, Jearl Walker

Articles:

[6] Bend It like Magnus: Simulating Soccer Physics/ Mohammad Ahmad (2011)

Modifications

1. All pages are numbered now.
2. All the notes has been corrected except some that are mentioned bellow

I. Page 2- table (1) and figure (3):
Explanation is in the paragraph before figure 3. Table 1 is only for clarifying figure 3 numbers of cylinders.

II. Page 5 equations (16) and (17):
"For these two equations, the authors simply copied the equations and the list-wise description of each physical quantity into the manuscript"
I don't understand what do you mean by copy and pasting equations.

III. "Page 6 -figure (7) and equation table:
Vectors are shown divided for clarifying the equations (20-27) because in equations these vectors have been used dividedly.
Equations should progress together with aim of reaching equations of motion in horizontal and vertical component at the same time.

IV. Page 6 predicted diagram:

(3) Line 2 – 6: The whole description, "The object …….before collision with ground.", can be used to describe any kind of projectile motion. What is the difference between the glider motion and the projectile motion, after the authors also took lift and drag forces into consideration in the calculation?"
it is a prediction graph based on theories that the glider will move like a projectile movement but not exactly the same and the result is in page 9 (Fig 12) where prediction and experiments are compared.

V. Page 8 "(3) the authors are very kind to list quite a few related parameters and possible sources of errors, including their description. But how do they fit into their results, that is, their calculated and recorded trajectories?"

They are mostly observed in calculations and experiments and they are mentioned for further researches that may be done by others so they will know what can be their errors.

2015 Problem 6 : Magnus glider

Experimental verification of the photoacoustic model

NISHANT VERMA
Anglo-Chinese School (Independent)
96.nishant@gmail.com

Abstract

No experimental verification in real units exits for the photoacoustic model for solids. Many papers have made photoacoustic measurements in arbitrary or relative units. This paper details the experimental set-up and procedure required to obtain experimental data of the photoacoustic phenomenon for solids in real units of sound intensity (Wm^{-2}) . The key assumptions made in the derivation of the photoacoustic model for solids have been highlighted and experimentally satisfied to obtain good agreement between theory and empirical data. Empirical data obtained in real units follow both the general trend and the exact values predicted by the photoacoustic theory. This paper also takes into theoretical consideration heat transfer from the sample to the air through both radiation and conduction.

1. Introduction

Alexander Graham Bell discovered the photoacoustic effect in 1880 when he observed that thin disks of many different materials emitted sounds when exposed to the action of a rapidly interrupted beam of sunlight [1]. In this investigation, the photoacoustic effect is reproduced by exposing a jar made of acrylic, coated on the inside with soot, to an incandescent lamp powered by alternating current (AC). A distinct sound is produced and is investigated both in terms of its intensity and frequency.

The photoacoustic effect has prominent applications in photoacoustic spectroscopy. Photoacoustic spectroscopy is used to study the properties of materials not accessible to optical spectroscopy, such as amorphous compounds, smears, gels and oils [2]. The solids and gases can be identified by the unique sound waves they produce when electromagnetic radiation energy is incident on a sample of the material.

Rosencwaig and Gersho derived the theory for photoacoustic effect for solids in one dimension in 1976 [3]. However, no verification of the model in absolute units exists, all experiments have been done in relative or arbitrary units [2, 4-7]. This article details the experiments conducted to verify the photoacoustic model for solids in real units of Wm^{-2}. This article also considers the relative significance of conduction and radiation as heat transfer mechanisms in the photoacoustic model. The theoretical model section shall focus on highlighting the key assumptions made in the theoretical derivation, which have to be experimentally reproduced, and the approximation made to apply the 1 dimensional model to the case of a 3 dimensional jar.

2.Theoretical model

2.1 Theoretical model overview

A lamp powered by AC has a modulating light intensity output that oscillates at twice the frequency of the AC supplied to the lamp. Each AC cycle has 2 “on” phases and 2 “off” phases that correspond to the doubled frequency. During the “on” phase of the AC cycle, light from the lamp is incident on the surface of the soot. The soot absorbs the light energy and heats up. During the “off” phase of the AC cycle, heat from the soot transfers to the air in the jar mainly by conduction (radiation is considered in subsection 2.5). The heated air in the jar expands, producing a pressure wave. This cycle repeats and the periodic expansion and contraction of the air in the jar produces a sound pressure wave that oscillates at the same frequency as the oscillation of the light intensity from the lamp. The sound wave tends to lag the light wave by a constant phase angle [3].

The theoretical model has been presented in three subsections, the first models the incidence of the light on the soot, the second solves for the temperature field in the jar and the last uses the temperature field of the jar

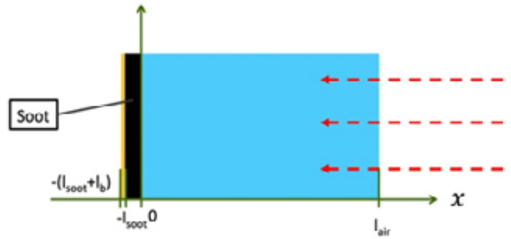

Figure 2.1.1: Cartesian coordinate system of the jar. The arrows indicate the direction of incoming light. From right to left: the first layer is the air in the jar, the second layer is the layer of soot and the last layer is the backing of the jar.

to calculate the intensity of the acoustic signal produced. The Cartesian coordinate system shown in figure 2.1.1 is used. l_{air} is the length of the air in the one-dimensional jar, l_{soot} is the length of the layer of soot and l_b is the length of the jar’s backing.

2.2 Incident light

The light intensity incident on the soot is given by

$$I=\frac{1}{2}I_{AC}(1+\cos\omega t) \tag{1}$$

Where I_{AC} is defined as twice the amplitude of the AC component of the light intensity incident on the soot. ω is the frequency of oscillation of the light intensity and t is time. Defining β as the optical absorption coefficient, a measure of the rate of decrease in the intensity of electromagnetic radiation as defined by the beer lambert law, the following equation is derived.

$$\frac{dI}{dx}=-\beta I \tag{2}$$

gives the following expression for light intensity absorbed per unit length of the soot

$$H=\frac{1}{2}I_{AC}\beta e^{\beta x}(1+\cos\omega t) \tag{3}$$

2.3 Temperature field

Heat transfers from the soot to the air mainly by conduction. Radiation accounts for less than 0.8% of the heat transfer (shown in subsection 2.5) and is thus neglected. It is also assumed that the air in the jar is not directly heated by the light from the lamp, this is a justified assumption considering the low optical absorption coefficient of air [8]. The following heat conduction equations are set-up for the soot

$$\frac{1}{k_{soot}}H+\frac{\partial^2\theta_{soot}}{\partial x^2}=\frac{1}{\alpha_{soot}}\frac{\partial\theta_{soot}}{\partial t} \tag{4}$$

the jar backing

$$\frac{\partial^2\theta_b}{\partial x^2}=\frac{1}{\alpha_b}\frac{\partial\theta_b}{\partial t} \tag{5}$$

and the air in the jar

$$\frac{\partial^2\theta_{air}}{\partial x^2}=\frac{1}{\alpha_{air}}\frac{\partial\theta_{air}}{\partial t} \tag{6}$$

Where θ is temperature, $\alpha_i=\frac{k_i}{\rho_i c_i}$ is the thermal diffusivity, ρ_i is the density, c_i is the specific heat capacity and k_i is the thermal conductivity of material i. The first additional term in the soot heat conduction equation arises from the heat energy generated from the absorption of the incoming light by the soot.

Six boundary conditions are required to solve the above three second order differential equations. The following boundary conditions are applied: temperature continuity at the air-soot boundary

$$\theta_{air}(0,t)=\theta_{soot}(0,t) \tag{7}$$

Temperature continuity at the soot-backing boundary

$$\theta_{soot}(-l_{soot},t)=\theta_b(-l_{soot},t) \tag{8}$$

Heat flux continuity at the air-soot boundary

$$k_{air}\frac{\partial\theta_{air}}{\partial x}(0,t)=k_{soot}\frac{\partial\theta_{soot}}{\partial x}(0,t) \tag{9}$$

Heat flux continuity at the soot-backing boundary

$$k_{soot}\frac{\partial\theta_{soot}}{\partial x}(-l_{soot},t)=k_b\frac{\partial\theta_b}{\partial x}(-l_{soot},t) \tag{10}$$

In addition, the temperature of the edges of the backing and air layer are set at the temperature of the surrounding as $\theta=T_0$

$$\theta_{air}(-l_{air},t)=T_0 \tag{11}$$

$$\theta_b(-(l_{soot}+l_b),t)=T_0 \tag{12}$$

The last two boundary conditions have to be satisfied experimentally by ensuring that a lamp of high wattage is not used and that the lamp is placed a certain distance away from the jar. This is to prevent the lamp from heating up the front surface of the jar, which would act as another source of heat generation. The experiment can also only be conducted over short durations to minimise the heating of the front and back surfaces of the jar.

Solving the differential equations yields the following expression for the temperature field of the air layer as a function of position and time:

$$\theta_{air}(x,t)=\left(1-\frac{x}{l_{air}}\right)\psi_0+\psi e^{-a_{air}x}e^{i(\omega t-a_{air}x)} \tag{13}$$

The first term represents the DC part of the solution while the second term represents the AC part. $e^{-a_{air}x}$ denotes the attenuation of temperature with distance from the surface of the soot and $e^{i(\omega t-a_{air}x)}$ denotes the periodic variation in air temperature. The complex amplitude ψ is defined as

$$\psi=\frac{\beta I_{AC}}{2k_{soot}\{\beta^2-[(1+i)a_{soot}]^2\}}\left[\frac{(r-1)(b+1)e^{(1+i)a_{soot}l_{soot}}-(r+1)(b-1)e^{-(1+i)a_{soot}l_{soot}}+2(b-r)e^{-\beta l_{soot}}}{(g+1)(b+1)e^{(1+i)a_{soot}l_{soot}}-(g-1)(b-1)e^{-(1+i)a_{soot}l_{soot}}}\right] \tag{14}$$

where r, g and b are further defined

$$r=(1-i)\frac{\beta}{2a_{soot}} \quad (15)$$

$$g=\frac{k_{air}a_{air}}{k_{soot}a_{soot}} \quad (16)$$

$$b=\frac{k_b a_b}{k_{soot}a_{soot}} \quad (17)$$

Where $a_i=\left(\frac{\omega}{2\alpha_i}\right)^{\frac{1}{2}}$ is the thermal diffusion coefficient of material *i*.

This full solution for ψ requires no assumptions about the properties of the material of the sample, backing or air. Taking into consideration the special properties of soot, acrylic and air, the full solution of ψ can be approximated. The first property of soot is that it is optically opaque [9]

$$e^{-\beta l_{soot}} \quad 0 \quad (18)$$

To satisfy this approximation in the experiment, the layer of soot cannot be too thin, such that light passes through the soot. The second property is that soot is thermally thin [10]

$$\left|e^{\pm(1+i)a_{soot}l_{soot}}\right|\cong 1 \quad (19)$$

the length of the soot is small in comparison to the wavelength of the heat wave that travels through the soot. This approximation is satisfied when the length of the soot layer is not extremely thick. A soot length of 0.5-1

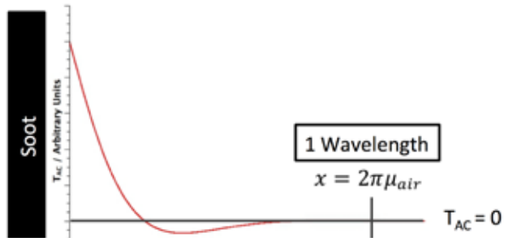

Figure 2.4.1: Graph of AC-part of temperature fluctuation of the air in the jar against distance from the soot surface.

mm will satisfy both approximations. With the further approximations $|r|\gg 1$ and $b<g$, the full solution for ψ is approximated to

$$\psi=\frac{(1-i)I_{AC}\sqrt{2k_b}}{4k_b\sqrt{\omega\rho_b c_b}} \quad (20)$$

2.4 Acoustic signal

Using the temperature field of the air layer derived in the previous subsection, the ideal gas law can be used to calculate the pressure fluctuations in the jar as a function of time and thus the acoustic signal produced.

The graph in figure 2.4.1 is obtained when the AC-part of equation (13) is plotted as a function of *x*. $\mu_i=\frac{1}{a_i}$ is the thermal diffusion length of material *i*.

The AC fluctuations in temperature quickly attenuate with distance from the soot. Within one thermal wavelength ($x=2\pi\mu_{air}$), the AC fluctuations in temperature attenuate to almost zero. An acoustic piston the length of one wavelength can be defined to be the only part of the layer of air that responds thermally to the AC temperature fluctuations at the surface of the soot, the acoustic piston is illustrated in figure 2.4.2. The acoustic piston expands and contracts in response to the temperature fluctuations at the surface of the soot. The rest of the air in the jar responds to this acoustic piston by bulk expansion and contraction. For suitable jar dimensions, the air in the jar could respond to the acoustic piston through the creation of longitudinal or radial standing waves, the theoretical model would not apply to such situations. To verify that standing waves were not set-up in the jar under investigation, the sound field in the jar was mapped by taking sound measurements at various positions in the jar, results are shown in Appendix [A]. The readings were constant at varying positions, suggesting constant pressure fluctuation throughout the jar and thus no standing waves.

The spatial average of the AC temperature of the acoustic piston is given by

$$\overline{\theta_{air}}(t)=\frac{1}{2\pi\mu_{air}}\int_0^{2\pi\mu_{air}}\theta_{AC}(x,t)dx \quad (21)$$

Approximating $e^{-2\pi}\ll 1$

$$\overline{\theta_{air}}(t)\cong\frac{1}{2\sqrt{2}\pi}\psi e^{i(\omega t-0.25\pi)} \quad (22)$$

The displacement of the piston as a function of time can be found by applying the ideal gas law

$$\frac{\delta x(t)}{2\pi\mu_{air}}=\frac{\overline{\theta_{air}}(t)}{T_0} \quad (23)$$

Where T_0 is the average DC temperature of the acoustic piston and is taken to be the DC temperature of the surface of the soot at $x=0$. This can be approximated to ambient temperature if the experiment is conducted over extremely short durations (10 – 20 s) with a low wattage lamp (< 60 watts). Rearranging and substituting

$$\delta x(t)=\frac{\psi\mu_{air}}{\sqrt{2}T_0}e^{i(\omega t-0.25\pi)} \quad (24)$$

Having eliminated the possibility of standing waves, bulk expansion and contraction of the rest of the air in the jar can be considered. Since the time of expansion and contraction of the acoustic piston is short, the process can be assumed to be adiabatic

$$\delta P=-\frac{\gamma P}{V}\delta V \quad (25)$$

Where *P* is the ambient pressure in the jar, taken to be the atmospheric pressure. Substituting $V=\pi R^2 h$ as the volume of the jar, where *R* is the radius and h is the height of the jar, and approximating $\delta V=\pi R h$"

$$\delta P=-\frac{\gamma P}{\pi R^2 h}(\pi R h)\delta x \quad (26)$$

The approximation $\delta V=\pi R h$ holds true for any arbitrary shape of the jar's surface as long as the length of the acoustic piston is much smaller than the radius of the jar. This approximation allows the one-dimensional model to be applied to a three-dimensional jar. Substituting equation (24) into equation (26):

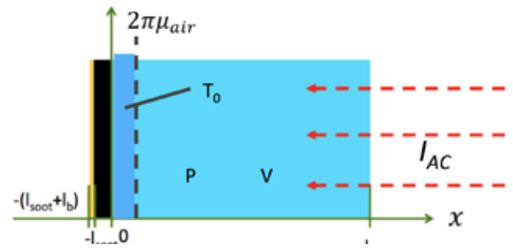

Figure 2.4.2: Schematic of a one-dimensional jar. The dark blue region denotes the acoustic piston while the light blue region denotes the rest of the air in the jar that responds to the acoustic piston by bulk expansion and contraction. P is the ambient pressure in the jar and V is the volume of the jar. T0 is the average DC temperature of the acoustic piston which is set as the DC temperature of the layer of soot at *x*=0 .

$$\delta P(t)=-\frac{\gamma P}{R}\frac{\psi\mu_{air}}{\sqrt{2}T_0}e^{i(\omega t-0.25\pi)} \quad (27)$$

The absolute value of equation (27) gives the amplitude of the sound pressure variation (P_{max}) in the jar. The sound intensity can be further calculated using

$$I_{sound}=\frac{(P_{max})^2}{2\rho_a v} \quad (28)$$

Where *v* is the velocity of sound in air, a function of T_0 and *P*. Substituting the absolute value of equation (27) into equation (28):

$$I_{sound}=\frac{1}{8}\frac{P^2I^2}{T_0^2\omega^2}\frac{k_{air}\gamma^2}{\rho_{air}^2\rho_b c_{air}c_b v R^2 k_b} \quad (29)$$

Equation (29) is the final expression for sound intensity produced in the jar as a function of the relevant parameters.

2.5 Heat transfer by conduction and radiation

Air is known to have a high emissivity value of $\epsilon\approx 0.84$ to long-wave radiation [11]. Radiation is thus a possible mechanism for heat transfer from the soot to the air layer. Theoretical calculations for heat flow by radiation ($H_{radiation}$) and conduction ($H_{conduction}$) were done to investigate the relative significance of radiation and conduction as heat transfer mechanisms.

Heat flow by conduction is given by

$$H_{\text{conduction}} = k_{\text{air}} A \frac{\partial \theta_{\text{air}}}{\partial x}(0,t) \quad (30)$$

Substituting

$$H_{\text{conduction}} = k_{\text{air}} A \psi a_{\text{air}} \sqrt{2} = 7.15 \times 10^{-3} \text{ Watts at cycle peak} \quad (31)$$

Similarly heat flow by radiation is given by

$$H_{\text{radiation}} = \epsilon \sigma A (T^4_{\text{SCOOT}} - T^4_{\text{air}}) \quad (32)$$

Substituting with $Q = m_{\text{soot}} c_{\text{soot}} \Delta T$

$$H_{\text{radiation}} = \epsilon \sigma A \left[\left(T_0 + \frac{Q}{m_{\text{soot}} c_{\text{soot}}} \right)^4 - T_0^4 \right] = 2.93 \times 10^{-5} \text{ Watts at cycle peak} \quad (33)$$

Comparing the relative significance of heat flow by conduction to heat flow by radiation

$$\frac{H_{\text{radiation}}}{H_{\text{conduction}}} \times 100\% = 0.8\% \quad (34)$$

Heat transfer by radiation is less than 0.8% of the heat transfer by conduction; this justifies neglecting heat transfer by radiation from the soot to the air layer.

3. Experimental design

3.1 General experimental set-up

The photoacoustic phenomenon was reproduced using a cylindrical jar with R=3.50 cm , h=20.0 cm and a ≈ 40 W incandescent lamp powered by AC, figure 3.1.1 depicts the cylindrical jar used. A jar with a large radius was chosen to satisfy the approximation in equation (26). It should be noted that h does not affect the intensity or frequency of the sound produced by the photoacoustic phenomenon for the geometry of a cylindrical jar.

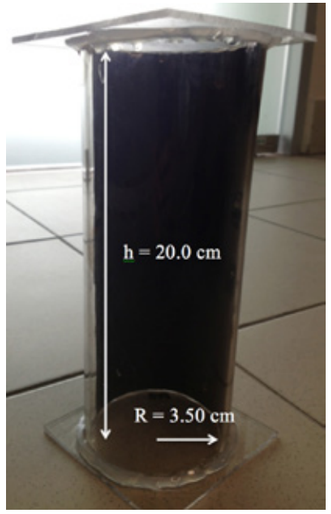

Figure 3.1.1: Cylindrical jar used for investigation. The jar was constructed with acrylic.

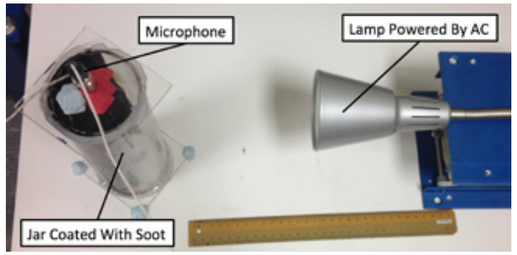

Figure 3.1.2: Picture of experimental set-up.

Half the inside of the jar was coated with an even layer of soot that absorbed the incident light from the lamp. The soot was coated using a lighter with butane fuel. The soot was coated onto the jar till light from a lamp positioned behind the jar was no longer visible through the soot. This was done to obtain an even coat of soot.

A hole of 8 mm diameter was made in the top of the jar to insert a microphone into the jar. The jar was then sealed to satisfy the adiabatic assumption made in equation (25). A Bruel & Kjaer 4138-A-015 microphone was used to make sound measurements. The microphone was calibrated with a Bruel & Kjaer calibration sound box at 94 dB at 1000 Hz prior to experimentation. This allowed for precise measurements of sound intensity in real units.

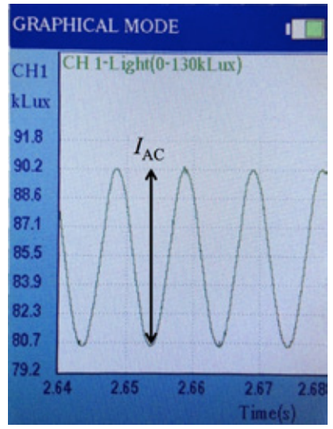

Figure 3.2.1: Sample waveform from lux meter sampling at 20,000 samples/s. Peak to peak reading is equal to IAC.

The experimental set-up is depicted in figure 3.1.2. The jar was placed at a fixed distance and orientation from the lamp. The lamp was also fixed in place throughout the experiment.

3.2 Light intensity

Light intensity was measured using a lux meter sampling at 20,000 samples/s. This allowed precise measurements of I_{AC}, which has a frequency of 100 Hz. A picture of the sample waveform from the lux meter is shown in figure 3.2.1.

To measure the light intensity incident on the surface of the soot, the absorption, reflection and lensing effect of the acrylic jar has to be taken into account. As such, the light intensity incident on the back of the jar was mapped (figure 3.2.2) using the lux meter and numerically integrated with respect to ϕ (figure 3.2.3) to obtain the total light intensity incident on the surface of the jar.

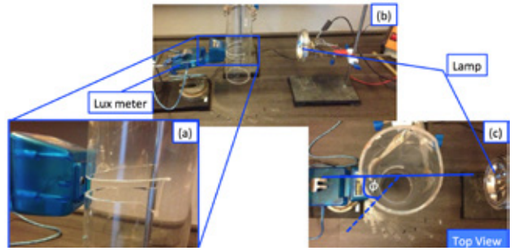

Figure 3.2.2: Process of mapping light intensity at the back of the jar. A jar with the same radius and material as the one used for investigation of the photoacoustic effect was constructed.
In place of the soot at the back of the jar, a slit was cut out.
A lux meter was then used to measure the light intensity at different angles ϕ from the horizontal.
Slit cut out in place of the soot, to measure light intensity that would otherwise be incident on the surface of the soot
Entire set-up used to map light intensity at the back of the jar
Angle ϕ from the horizontal (solid blue line), 0-90°, symmetrical about the horizontal.

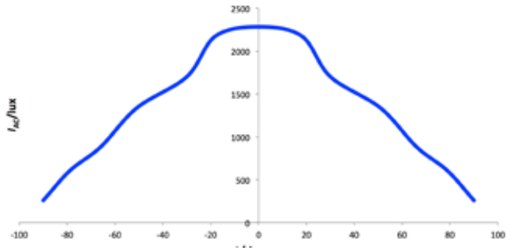

Figure 3.2.3: Graph of I_{AC} against ϕ, the graph is numerically integrated with respect to ϕ to obtain the total light intensity incident on the surface of the soot. Error in measurement of I_{AC} is 4%.

The lux meter only measures light intensity in the visible region. However, a large part of the radiation from the incandescent lamp is in the infrared spectrum. To correct for this, the electrical power delivered to the lamp was measured using multimeters. It was assumed that all the energy input into the lamp is converted to electromagnetic radiation and that the lamp filament acts as a black body, a suitable assumption considering the high temperature of the filament. The lux meter is known to measure the electromagnetic radiation for a particular frequency range. The Plank's law equation

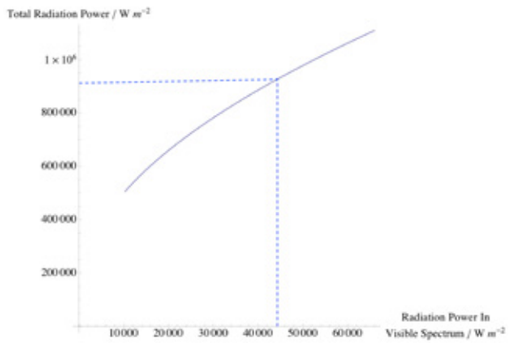

Figure 3.2.4: Graph of total radiation power against radiation power in the visible spectrum. This graph has not been calibrated.

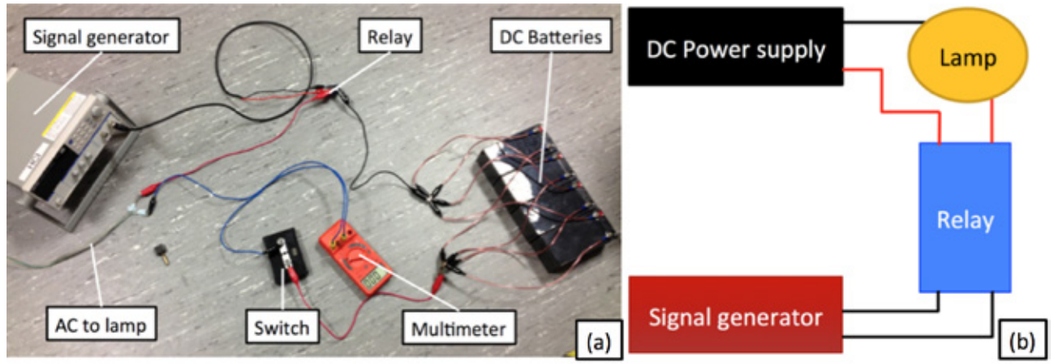

Figure 3.3.1: (a) – Schematic and (b) picture of experimental set-up to vary light chopping frequency.

can be integrated for that particular frequency range with respect to f and used to convert between power emitted in the visible region to power emitted across the whole electromagnetic spectrum, this is depicted graphically in figure 3.2.4. The temperature of the filament at a certain electrical power input has to be known to calibrate the curve.

Light intensity was varied by placing two polarises between the lamp and the jar and by rotating the relative orientation of the two polarisers. The light intensity was remapped and reprocessed for the different orientations of the polariser.

3.3 Frequency of oscillation of light intensity

The frequency of oscillation of light intensity or light chopping frequency was controlled using a signal generator connected to a relay. The light frequency output from the lamp was then verified using the lux meter sampling at 20,000 Hz. An electrical circuit was set-up to control the chopping frequency of the lamp. A signal generator was connected to a relay, causing the relay to open and close at a controlled number of times per second. The output pins of the relay were connected in series with a DC power supply to the lamp, thus controlling the chopping frequency of the lamp, producing an approximately sinusoidal waveform. A schematic and picture of the electrical circuit is shown in figure 3.3.1.

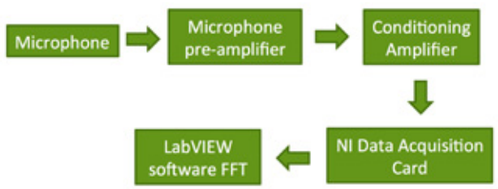

Figure 3.4.1: Processing of audio signal for photoacoustic measurements.

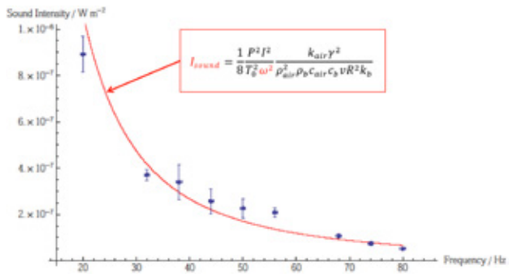

Figure 4.1: Graph of sound intensity against light chopping frequency. Red line is the theoretical plot. Blue data points are empirical.

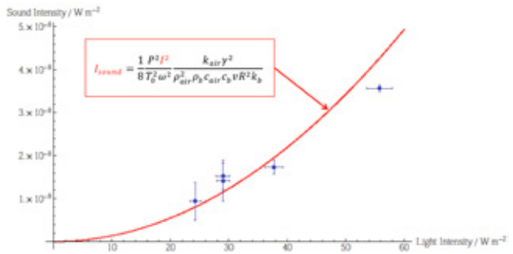

Figure 4.2: Graph of sound intensity against light intensity. Red line is the theoretical plot. Blue data points are empirical.

3.4 Data collection and processing

Figure 3.4.1 depicts the processing of the audio signal in the form of a flow chart. The microphone sampled at 40 kHz for 10 s. A Bruel & Kjaer conditioning amplifier compatible with the microphone was used. The time-amplitude signal was processed by the FFT algorithm in the LabVIEW software to give an amplitude-frequency list. The peak amplitude was located and the amplitude-frequency graph was numerically integrated with respect to frequency from 0.5 Hz below to 0.5 Hz above the peak frequency, this range was sufficient to capture the sound signal produced by the photoacoustic effect.

4.Results

The theoretical values used in figure 4.1 and 4.2 are given in table 4.1, all values were theoretically or experimentally measured.

Table 4.1 Numerical values used for theory plot.

Symbol	Description	Value
ρ_a	Density of air	1.18 kg m^{-3}
ρ_b	Density of acrylic backing	1200 kg m^{-3}
C_a	Specific heat capacity of air	1055 J kg^{-1} k^{-1}
C_b	Specific heat capacity of acrylic backing	1297 J kg^{-1} k^{-1}
v	Velocity of sound in air	347 m s^{-1}
k_a	Thermal conductivity of air	0.0271 W m^{-1} k^{-1}
k_b	Thermal conductivity of acrylic backing	0.152 W m^{-1} k^{-1}
T_0	Ambient temperature	298 K
P	Ambient pressure	101000 Pa
R	Radius of jar	3.50 cm
γ	Adiabatic constant of air	1.4
ω	Light chopping frequency (figure 4.2 only)	100 Hz
I_{AC}	Light intensity (figure 4.1 only)	55.8 W m^{-2}

5. Discussion

Having closely followed all the assumption made in the theoretical model, a good agreement is observed between experiment and theory. Empirical data obtained in real units follow both the general trend and the exact values predicted by theory.

As the chopping frequency is increased, there is less time for heat to transfer from the soot to the air in the jar, thus the amount of heat transferred is less and the corresponding expansion of the air is less. These smaller pressure fluctuations mean a lower sound intensity. Similarly, when the incoming light intensity is increased, the soot heats up to a greater degree and more heat energy is transferred from the soot to the air in the jar and the air expands to a greater extent, resulting in greater pressure fluctuations and a larger sound intensity reading.

The theory is expected to deviate from experiment at much larger light intensity values when the light from the lamp directly heats up the front of the jar, violating the $\theta = T_o$ boundary condition at $x=l_{air}$ When this occurs the front of the jar will act as another source of heat and the boundary conditions and heat conduction equations can be adapted to model the scenario.

The theoretical model overview indicates that the photoacoustic theory will be observed regardless of the material of the solid backing of the jar or the fluid in the jar. The intensity of sound produced may be significantly decreased based on the absorbance of light by the fluid as the light travels towards the solid backing. In fact, if the fluid absorbs a significant portion of the light, the mechanism of sound production might shift from heating and cooling of the fluid medium directly rather than indirectly through the backing material. The above mathematical model would be incomplete for non-ideal fluids such as water

due to the use of equation (23). The approximations made to reduce equation (20) to equation (14) might also not hold for certain backing materials and fluids.

6. Conclusion

The theory of the photoacoustic effect for solids has been reviewed and the key assumptions made in the theory that have to be experimentally reproduced to obtain accurate results have been highlighted. It has been theoretically shown that heat transfer from the soot to the air layer occurs mainly through conduction instead of radiation. A detailed description of the experimental procedures and set-up used to collect sound intensity readings in real values has been given. A good agreement between theory and experiment in absolute units of W m^{-2} was observed.

References

[1] A G Bell 1880 On the Production and Reproduction of Speech by Light American Journal of Science 20 305–324.

[2] A. Rosencwaig 1973 Photoacoustic spectroscopy of solids Optics Communications 7 305-8

[3] A. Rosencwaig and A. Gersho 1976 Theory Of The Photoacoustic Effect With Solids Journal of Applied Physics 47 64-9

[4] A. Rosencwaig 1978 Theoretical aspects of photoacoustic spectroscopy Journal of Applied Physics 49 2905-10

[5] B Baumann, M Wolff, B Kost and H Groninga 2007 Finite element calculation of photoacoustic signals Applied Optics 46 1120-25

[6] A Miklos, P Hess and Z Bozoki 2001 Application of acoustic resonators in photoacoustic trace gas analysis and metrology Review of Scientific Equipment 72 1937-55

[7] C A Bennett Jr and R R Patty 1982 Thermal wave interferometry: a potential application of the photoacoustic effect Applied Optics 21 49-54

[8] Y G Toporkov 1983 Laboratory investigation of the absorption coefficients of air at "λ=10.6 μm" Journal of applied spectroscopy 40 424-9

[9] K.M. Hamasha and W. P. Arnott 2009 Photoacoustic Measurements Of Black Carbon Light Absorption Coefficients In Irbid City, Jordan Environmental Monitoring and Assessment 166 485-94

[10] P E Khizhnyak, A V Chechetikin and A P Glybin 1979 Thermal Conductivity Of Carbon Black Journal of Engineering Physics and Thermal Physics 37 1073-75

[11] B Hodges 1998 Heat budget and thermodynamics at a free surface: some theory and numerical implementation (revision 1.0c) ED 1300 BH Centre for water research University of Western Australia 14

Appendix A

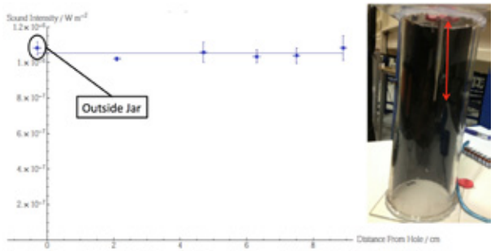

Figure a1: Graph of sound intensity against longitudinal distance from hole as measured by the red arrow. The constant sound intensity readings at varying longitudinal distances suggest constant pressure fluctuations and no presence of nodes or anti nodes. Hence, eliminating the possibility of standing waves in the jar.

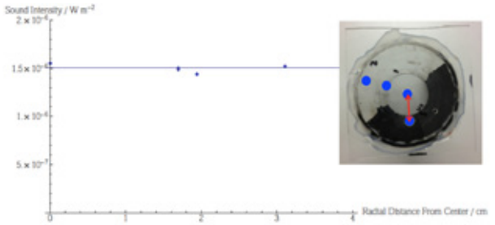

Figure a2: Graph of sound intensity against radial distance from hole as indicated by the blue dots and measured by the red arrow. The constant sound intensity readings at varying radial distances suggest constant pressure fluctuations and no presence of nodes or anti nodes. Hence, eliminating the possibility of standing waves in the jar.